Journal of Advanced Ceramics
2019, **8**(4): 576–582
https://doi.org/10.1007/s40145-019-0342-4
ISSN 2226-4108
CN 10-1154/TQ

Rapid Communication

High-entropy pyrochlores with low thermal conductivity for thermal barrier coating materials

Fei LI†, Lin ZHOU†, Ji-Xuan LIU, Yongcheng LIANG, Guo-Jun ZHANG*

State Key Laboratory for Modification of Chemical Fibers and Polymer Materials, *College of Materials Science and Engineering*, *Institute of Functional Materials*, *College of Science*, *Donghua University*, *Shanghai 201620*, *China*

Received: June 5, 2019; Accepted: June 18, 2019

Abstract: High-entropy pyrochlore-type structures based on rare-earth zirconates are successfully produced by conventional solid-state reaction method. Six rare-earth oxides (La_2O_3, Nd_2O_3, Sm_2O_3, Eu_2O_3, Gd_2O_3, and Y_2O_3) and ZrO_2 are used as the raw powders. Five out of the six rare-earth oxides with equimolar ratio and ZrO_2 are mixed and sintered at different temperatures for investigating the reaction process. The results demonstrate that the high-entropy pyrochlores $(5RE_{1/5})_2Zr_2O_7$ have been formed after heated at 1000 ℃. The $(5RE_{1/5})_2Zr_2O_7$ are highly sintering resistant and possess excellent thermal stability. The thermal conductivities of the $(5RE_{1/5})_2Zr_2O_7$ high-entropy ceramics are below 1 $W\cdot m^{-1}\cdot K^{-1}$ in the temperature range of 300–1200 ℃. The $(5RE_{1/5})_2Zr_2O_7$ can be potential thermal barrier coating materials.

Keywords: thermal barrier coating (TBC); pyrochlore; high-entropy ceramics; thermal conductivity

1 Introduction

Thermal barrier coating (TBC) materials are refractory ceramics with low thermal conductivity that are usually applied to metallic surfaces, such as on gas turbines or jet engines, to protect the metallic inner parts from overheating during long-term use [1–6]. To be an excellent TBC material, it requires low thermal conductivity, relatively high thermal expansion coefficient compatible with metallic substrate, high stability at elevated temperature, and good sintering resistance [1,4]. Yttrium stabilized zirconia (YSZ) is the state-of-the-art TBC material and has been chosen as the industry standard for last decades [4,7,8]. However, the accepted upper limit for YSZ during long-term use is 1200 ℃ due to its relatively high thermal conductivity and the metastable tetragonal phase degradation [9]. Great efforts have been devoted to explore new oxide compositions with low thermal conductivity and excellent thermal stability that can be considered as promising candidates in TBC applications [1]. Among the extensively studied refractory oxides, the rare-earth zirconates, i.e., the ternary metallic oxides ($RE_2Zr_2O_7$) with pyrochlore structure are important candidates [9,10]. The pyrochlores $RE_2Zr_2O_7$, where RE is one or multicomponent of lanthanides, exhibit lower thermal conductivity and excellent thermal stability comparable to YSZ, making them very promising TBC materials for application at temperatures above 1300 ℃ [9,10]. Defect engineering (e.g., vacancies, substitutions, and lattice distortion) has been proven to be an effective way to reduce the

†These authors contributed equally to this work.
* Corresponding author.
E-mail: gjzhang@dhu.edu.cn

intrinsic thermal conductivity of pyrochlores $RE_2Zr_2O_7$, aiming to a value below ~1 $W \cdot m^{-1} \cdot K^{-1}$ [9].

Very recently, the concept of high-entropy coming from high-entropy alloys has been brought to ceramics world [11,12]. Five or more components with equimolar or near equimolar ratio can be stabilized into a much simpler structure than expected. There are four core effects, namely high-entropy, severe lattice distortion, sluggish diffusion, and cocktail effects, in high-entropy materials that may affect their microstructure and properties [13]. High-entropy oxides [12], carbides [14,15], borides [16], and silicides [17,18] with rock salt structures or simple hexagonal structures and with fascinating properties have been produced by solid-state reactions and high temperature sintering. As for oxide ceramics, single-phase high-entropy rock salt (AO) [12], fluorite (AO_2) [19], perovskite (ABO_3) [20], and spinel (AB_2O_4) [21] structures, where A and B are metallic elements, have been established. However, to the best of our knowledge, there are no publications dealing with the high-entropy pyrochlores. High-entropy pyrochlores ($A_2B_2O_7$) with highly disordered and distorted structures and high average atomic weight are expected to exhibit low thermal conductivity at high temperatures, which makes them very attractive TBC candidates and needs investigation.

Recently, we have successfully synthesized high-entropy ceramic powders for thermal barrier coatings [22]. Here, in this work, we focused on the preparation and characterization of high-entropy pyrochlores based on ternary rare-earth zirconates ($RE_2Zr_2O_7$). Five lanthanides (La_2O_3, Nd_2O_3, Sm_2O_3, Eu_2O_3, and Gd_2O_3) and Y_2O_3 were selected as starting materials to make A sites in pyrochlore structure highly disordered, while keeping B sites unchangeable. By choosing five out of the six rare oxides with equimolar ratio, we successfully got six high-entropy pyrochlores. The thermal conductivity and thermal stability at elevated temperatures of these high-entropy pyrochlores were preliminarily investigated.

2 Experimental procedures

Y_2O_3 (99.99%, 5 μm) and La_2O_3 (99.95%, 8 μm) were purchased from Sinopharm Chemical Reagent Co., Shanghai, China. Nd_2O_3 (99.9%, 5 μm), Sm_2O_3 (99.9%, 8 μm), Eu_2O_3 (99.99%, 5 μm), and Gd_2O_3 (99.99%, 5 μm) were purchased from Shanghai Diyang Co., Shanghai, China. Monoclinic ZrO_2 (≥ 99.95%, 0.2 μm) was obtained from Zhuzhou Cemented Carbide Works Imp. & Exp. Co., Zhuzhou, China. All reagents were used as received. The high-entropy pyrochlores were prepared by solid-state reaction method. The molar ratio of the sum of total rare elements to zirconium was 1:1. Firstly, five of the six rare-earth oxides with equimolar ratio were mixed with ZrO_2 by planetary ball milling for 10 h at 560 r/min. The ground powder mixtures were cold isostatic pressed under 200 MPa and then sintered at different temperatures from 600 to 1500 ℃ for 1 h for investigating the formation process. The samples sintered at 1500 ℃ for 3 h were used to property characterization. In order to test their thermal stability at elevated temperatures, the as-sintered ceramics were aged at 1300 ℃ in air for 24 h. The as-sintered high-entropy ceramics were denoted as $(5RE_{1/5})_2Zr_2O_7$.

The phase structure of specimens was measured by X-ray diffraction (XRD, Bruker AXS D8 Discover, Germany) with Cu Kα radiation. Polycrystalline silicon powders were used as internal standard to calibrate the instrumental conditions. In each case, 0.1 g silicon powders were mixed with 1.0 g ceramic powders. The morphology and elemental distributions of the sintered ceramics were analyzed by a scanning electron microscope (FE-SEM, Hitachi, SU8010) equipped with energy dispersive spectrometry (EDS). The density of the sintered ceramics was determined by Archimedes method and the theoretical density (ρ) of each sintered ceramic was calculated using lattice parameters measured by XRD patterns. Thermal diffusivity α was measured by ultra-high temperature laser thermal conductivity meter (DLF-2800, TA Instruments, USA) in the temperature range from 300 to 1500 ℃. Specific heat capacity c_p was obtained by a thermal analyzer (MHTC 96, Setaram, KEP Technologies, France). Then the thermal conductivity κ of the sintered ceramics was calculated from the equation $\kappa = \alpha \times \rho \times c_p$.

3 Results and discussion

Figure 1(a) shows the XRD patterns of the mixtures of the raw powders (sample number 1#) and ceramic products after sintering at temperatures ranging from 600 to 1500 ℃. Diffraction peaks of the starting oxides can be detected in the mixtures of the raw powders and no new diffraction peaks are observed when heated at 600 ℃ for 1 h. When heated at 700 ℃, except for the raw starting oxides, weak diffraction peaks of $La_2Zr_2O_7$

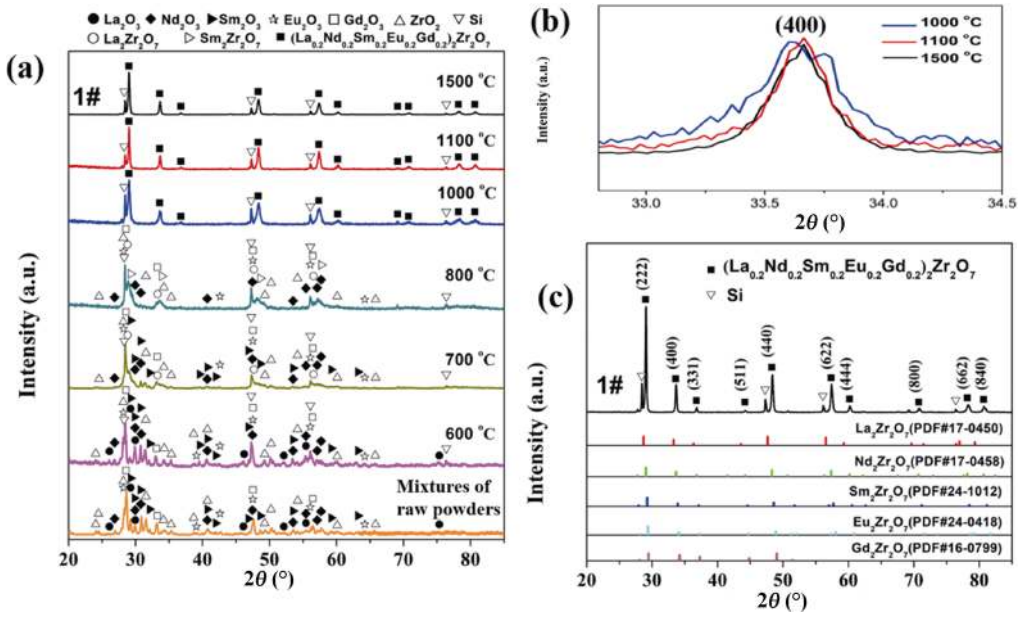

Fig. 1 (a) XRD patterns of the mixtures of raw powders (sample number 1#) and ceramic products after sintering at temperatures ranging from 600 to 1500 ℃. (b) Zoom-in view of the (400) diffraction peaks of the ceramics sintered at 1000, 1100, and 1500 ℃. (c) XRD patterns of ceramics 1# sintered at 1500 ℃ for 3 h.

can also be indexed, demonstrating the reaction between La_2O_3 and ZrO_2 occurs first at such low temperature. Upon increasing the heating temperatures, the intensity of the diffraction peaks of starting oxides decreases and diffraction peaks of $Sm_2Zr_2O_7$ appear at 800 ℃. The diffraction peaks of the ceramics sintered at 1000 ℃ can be indexed as a single-phase pyrochlore-type structure, which are featured with peaks at 2θ of 36.8° (331) and 44.2° (511) [10,23,24]. No obvious changes in the XRD patterns are observed when further increasing the heating temperatures to 1500 ℃, as clearly shown in Fig. 1.

Figure 1(b) shows a zoom-in view of the (400) diffraction peaks of the ceramics sintered at 1000, 1100, and 1500 ℃. The full width at half maximum of (400) peaks decreases with increasing heating temperatures, demonstrating the increased crystallinity of the sintered ceramics. The relative peak intensity ratio of silicon standard and the sintered ceramics decreases with the increase of heating temperatures, which also indicates increased crystallinity of the ceramics. Figure 1(c) shows the XRD patterns of ceramics 1# sintered at 1500 ℃ for 3 h. Standard JCPDS cards of $RE_2Zr_2O_7$ (RE = La, Nd, Sm, Eu, Gd) are provided for better understanding. The diffraction peaks of ceramics 1# can be indexed as a pyrochlore-type structure, but cannot be assigned to any ternary rare-earth zirconates. The XRD results confirm the formation of a novel single-phase high-entropy $(La_{0.2}Nd_{0.2}Sm_{0.2}Eu_{0.2}Gd_{0.2})_2Zr_2O_7$ with pyrochlore-type structure after sintering at 1000 ℃. The relatively low synthesis temperature should be important for the application of the high-entropy pyrochlores as TBC materials through such as thermal spray technology.

Figure 2(a) shows the XRD patterns of the ceramics after sintering at 1500 ℃ for 3 h. The diffraction peaks of these six sintered ceramics are similar to each other and all can be indexed as pyrochlore-type structure, even though they possess different compositions. This demonstrates the formation of single-phase high-entropy solid-solution structures among these rare-earth zirconates. Figure 2(b) illustrates one-eighth of the unit cell of the high-entropy pyrochlore structure with five different rare-earth ions randomly occupying rare-earth ion sites in $RE_2Zr_2O_7$ phase [9]. It is well known that the degree of structural disordering in $RE_2Zr_2O_7$ solid solutions is determined by the ionic radius ratio of rare-earth ions and zirconium ion [9]. Five equimolar light rare-earth elements are selected as starting materials in our cases, and the results demonstrate that the designed ceramics are in the stability field of the pyrochlore structure. By replacing rare-earth ions with Y^{3+} in sequence in ceramics 1# $(La_{0.2}Nd_{0.2}Sm_{0.2}Eu_{0.2}Gd_{0.2})_2Zr_2O_7$, the diffraction peaks of 2# shift to higher angle and then shift gradually to lower angle from ceramics 3# to 6#, as clearly shown in Fig. 2(c). Figure 2(d) shows the calculated lattice

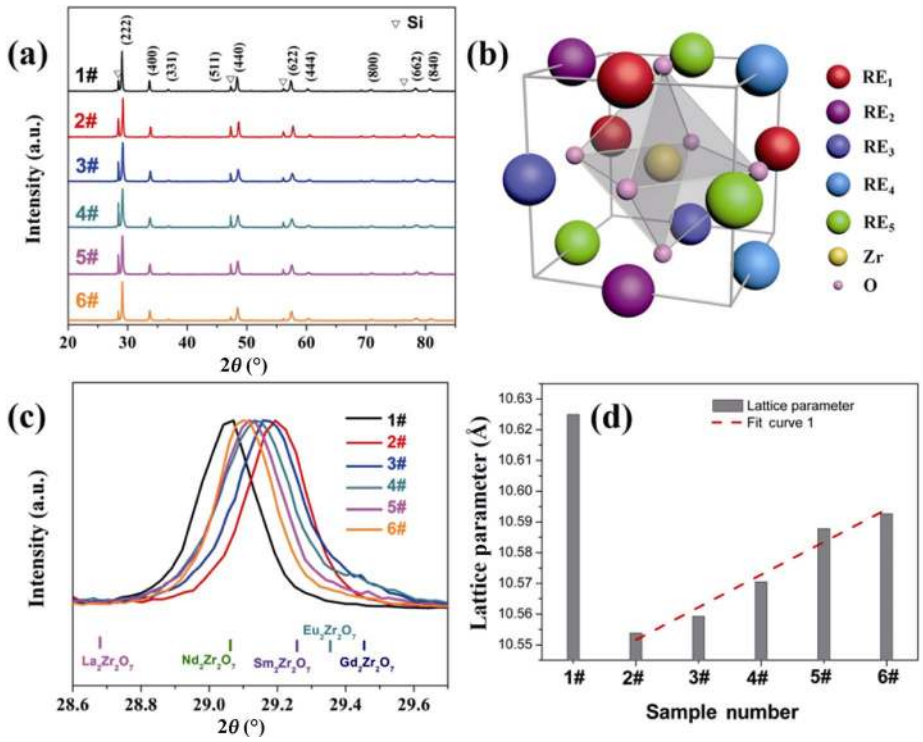

Fig. 2 (a) XRD patterns of the ceramics 1# $(La_{0.2}Nd_{0.2}Sm_{0.2}Eu_{0.2}Gd_{0.2})_2Zr_2O_7$, 2# $(Y_{0.2}Nd_{0.2}Sm_{0.2}Eu_{0.2}Gd_{0.2})_2Zr_2O_7$, 3# $(La_{0.2}Y_{0.2}Sm_{0.2}Eu_{0.2}Gd_{0.2})_2Zr_2O_7$, 4# $(La_{0.2}Nd_{0.2}Y_{0.2}Eu_{0.2}Gd_{0.2})_2Zr_2O_7$, 5# $(La_{0.2}Nd_{0.2}Sm_{0.2}Y_{0.2}Gd_{0.2})_2Zr_2O_7$, and 6# $(La_{0.2}Nd_{0.2}Sm_{0.2}Eu_{0.2}Y_{0.2})_2Zr_2O_7$ after sintering at 1500 ℃ for 3 h. (b) One-eighth of the unit cell of the high-entropy pyrochlore structure. (c) Zoom-in view of the (222) diffraction peaks of the sintered ceramics with various compositions. (d) Lattice parameters of the sintered ceramics.

constants of the sintered ceramics and the curve of the linear fit also is given for better understanding. Almost linear increase of the lattice parameters in sintered ceramics 2#, 3#, 4#, 5#, and 6# can be clearly observed. Such changes are reasonable due to that the larger rare-earth ions are substituted by smaller Y^{3+} [10].

The synthesis of high-entropy pyrochlore-type structured phases is almost complete at 1000 ℃; however, the densification of the ceramics requires higher sintering temperatures. The theoretical density of the high-entropy pyrochlores is calculated by using the molecular weight and the number of molecules per elementary cell [25]. The densities of these single-phase high-entropy pyrochlores after sintering at 1500 ℃ for 3 h are between 71% and 80% of the theoretical value, as listed in Table 1. The low relative densities might be due to the sluggish diffusion effect in the high-entropy pyrochlores caused by the presence of various cations [26]. Such an anti-sinterability should be beneficial to the performance of TBCs when facing a high temperature environment.

Figure 3 shows the fracture surface of the as-sintered ceramics (1# and 2#). The fracture surfaces of the as-sintered ceramics 1# and 2# are similar to each other, and they both possess grains in the submicron scale (~1 μm). The fracture mode of these ceramics is

Table 1 Theoretical density, relative density, and open porosity of the ceramics after sintering at 1500 ℃ for 3 h

Sample number	Nominal composition	Theoretical density ($g \cdot cm^{-3}$)	Relative density (%)	Open porosity (%)
1#	$(La_{0.2}Nd_{0.2}Sm_{0.2}Eu_{0.2}Gd_{0.2})_2Zr_2O_7$	6.554	71.4	28.9
2#	$(Y_{0.2}Nd_{0.2}Sm_{0.2}Eu_{0.2}Gd_{0.2})_2Zr_2O_7$	6.461	79.8	20.0
3#	$(La_{0.2}Y_{0.2}Sm_{0.2}Eu_{0.2}Gd_{0.2})_2Zr_2O_7$	6.427	76.5	23.5
4#	$(La_{0.2}Nd_{0.2}Y_{0.2}Eu_{0.2}Gd_{0.2})_2Zr_2O_7$	6.379	74.0	23.7
5#	$(La_{0.2}Nd_{0.2}Sm_{0.2}Y_{0.2}Gd_{0.2})_2Zr_2O_7$	6.341	73.9	22.8
6#	$(La_{0.2}Nd_{0.2}Sm_{0.2}Eu_{0.2}Y_{0.2})_2Zr_2O_7$	6.308	73.2	25.4

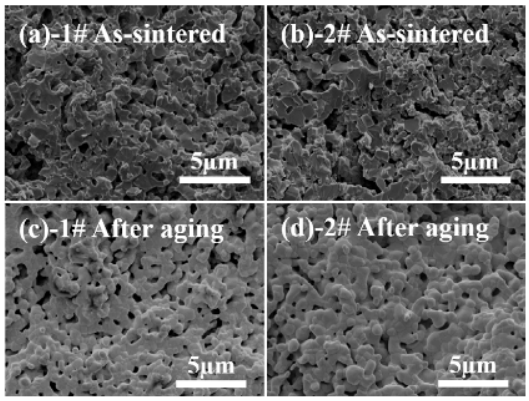

Fig. 3 Fracture surfaces of the ceramics (1# and 2#) before and after thermal aging at 1300 ℃ for 24 h.

predominantly transgranular fracture, demonstrating the relatively strong grain boundaries in the ceramics. The fracture surfaces of the other specimens (3#, 4#, 5#, 6#) and their corresponding thermal aged samples demonstrate very similar features (Fig. S1 in the Electronic Supplementary Material (ESM)).

In order to test the stability of the as-sintered ceramics at high temperature applications, the ceramics (1#–6#) are thermally aged at 1300 ℃ for 24 h. In general, 1300 ℃ is a kind of typical high temperature for TBC applications [1,7,27]. Figures 3(c) and 3(d) depict the fracture surface of the ceramics 1# and 2# after thermal aging. Thermal aging of the ceramics causes curving of the grains, which implies the grain boundaries are thermally etched. The grain sizes of the thermal aged samples do not show apparent changes, indicating the microstructures of the synthesized high-entropy ceramics are stable at this condition. The fracture surfaces of the ceramics (3#–6#) after thermal aging are shown in Fig. S1 in the ESM. The XRD patterns of the ceramics (1#–6#) after thermal aging can be assigned to pyrochlore-type structure and do not show obvious changes compared with the as-sintered ceramics, as shown in Fig. S2 in the ESM. All the results confirm that these single-phase high-entropy pyrochlores are sintering resistant and exhibit excellent high temperature stability and durability.

Figure 4 shows the elemental mappings of the single-phase high-entropy ceramics (1#–6#). The rare-earth, zirconium, and oxygen elements are uniformly distributed, indicating that all the as-sintered ceramics are chemically homogeneous.

Thermal conductivity is one of the key properties for TBCs [1,3,4,27]. Many strategies (e.g., substitution and vacancy formation) have been applied for reducing the thermal conductivity of TBCs [9,28]. Figure 5 shows the thermal conductivity of the single-phase high-entropy pyrochlore-type structures at temperatures ranging from 300 to 1500 ℃. In almost all samples, the thermal conductivities increase with the increasing temperature.

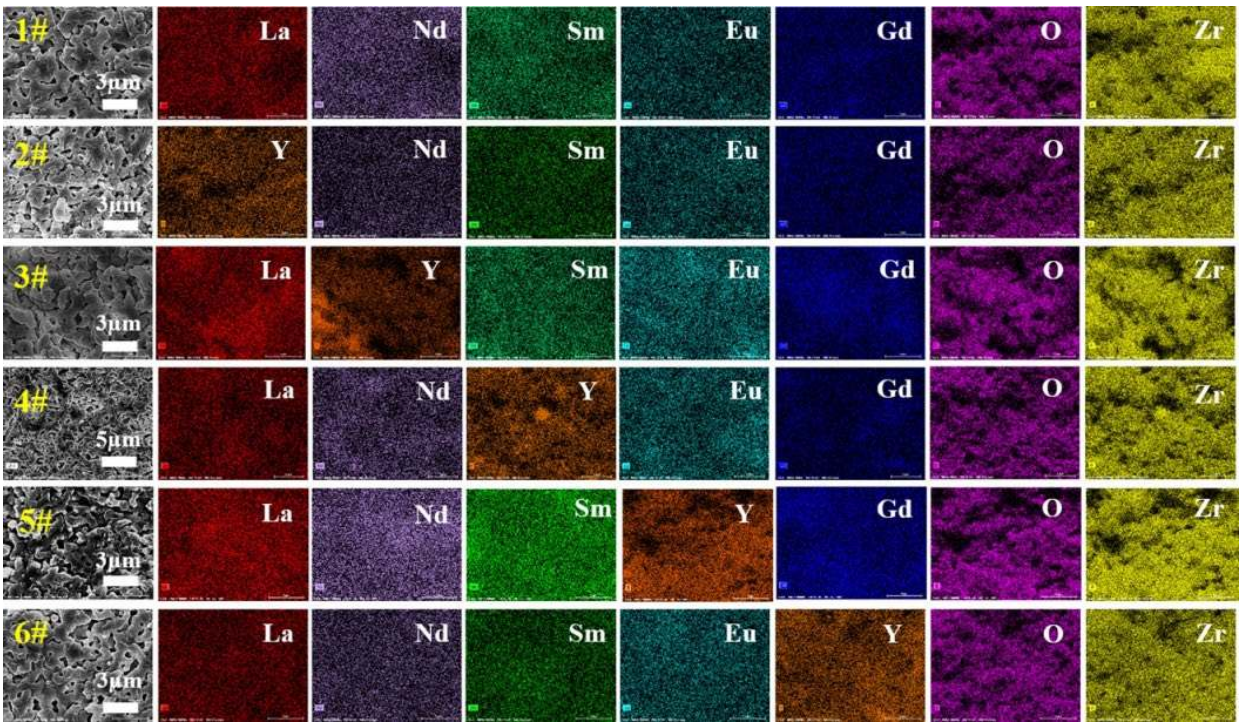

Fig. 4 Elemental mappings of the ceramics (1#–6#) after sintering at 1500 ℃ for 3 h.

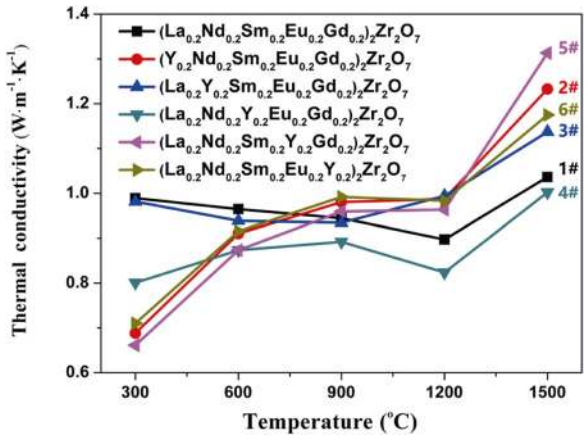

Fig. 5 Thermal conductivity as a function of temperature for the ceramics (1#–6#) after sintering at 1500 ℃ for 3 h.

The thermal conductivity values are below 1 $W \cdot m^{-1} \cdot K^{-1}$ from 300 to 1200 ℃, which is nearly 50% lower than that of the state-of-the-art TBC (yttria stabilized zirconia) with similar porosity levels [9]. High-entropy pyrochlores can be considered as solid solutions that five equimolar rare-earth cations randomly occupy the same lattice crystallographic sites in pyrochlore structure. The mass and radius mismatch of the cations result in great lattice distortion and strong phonon scattering in materials. Lattice distortion, one of the four so-called core effects in high-entropy materials, might be one of the main reasons that resulting in the reduced thermal conductivities of these single-phase high-entropy pyrochlores [26]. However, more specific reasons for single-phase high-entropy pyrochlores with reduced thermal conductivities are still under investigation.

4 Conclusions

In summary, single-phase high-entropy pyrochlores $(5RE_{1/5})_2Zr_2O_7$ based on rare-earth zirconates have been successfully produced by solid-state reactions between rare-earth oxides and zirconia. The formation of $(5RE_{1/5})_2Zr_2O_7$ is complete at 1000 ℃. The relative densities of these $(5RE_{1/5})_2Zr_2O_7$ are in the range of 70%–80% after sintering at 1500 ℃, which might be ascribed to the sluggish diffusion of high-entropy materials. The thermal conductivities of $(5RE_{1/5})_2Zr_2O_7$ are below 1 $W \cdot m^{-1} \cdot K^{-1}$ from 300 to 1200 ℃. These $(5RE_{1/5})_2Zr_2O_7$ are highly sintering resistant and exhibit excellent thermal stability, which makes them very promising TBC candidate materials and requires further investigation.

Acknowledgements

Financial support from the National Natural Science Foundation of China (Nos. 51532009, 51602324, and 51872405) are gratefully acknowledged.

Electronic Supplementary Material

Supplementary material (fracture surfaces of the ceramics (3#–6#) before and after thermal aging; XRD patterns of the ceramics (1#–6#) after thermally aging at 1300 ℃ for 24 h) is available in the online version of this article at https://doi.org/10.1007/s40145-019-0342-4.

References

[1] Pan W, Phillpot SR, Wan CL, *et al*. Low thermal conductivity oxides. *MRS Bull* 2012, **37**: 917–922.
[2] Padture NP, Gell M, Jordan EH. Thermal barrier coatings for gas-turbine engine applications. *Science* 2002, **296**: 280–284.
[3] Vaßen R, Jarligo MO, Steinke T, *et al*. Overview on advanced thermal barrier coatings. *Surf Coat Technol* 2010, **205**: 938–942.
[4] Clarke DR, Phillpot SR. Thermal barrier coating materials. *Mater Today* 2005, **8**: 22–29.
[5] Vassen R, Cao XQ, Tietz F, *et al*. Zirconates as new materials for thermal barrier coatings. *J Am Ceram Soc* 2004, **83**: 2023–2028.
[6] Guo W, Ma S, Liu L, *et al*. CMAS corrosion and protection of thermal barrier coatings for aeroengine. *Adv Ceram* 2017, **38**: 159–175. (in Chinese)
[7] Liu B, Liu YC, Zhu CH, *et al*. Advances on strategies for searching for next generation thermal barrier coating materials. *J Mater Sci Technol* 2019, **35**: 833–851.
[8] Chen L, Yang G-J. Epitaxial growth and cracking of highly tough 7YSZ splats by thermal spray technology. *J Adv Ceram* 2018, **7**: 17–29.
[9] Zhao M, Pan W, Wan CL, *et al*. Defect engineering in development of low thermal conductivity materials: A review. *J Eur Ceram Soc* 2017, **37**: 1–13.
[10] Yang L, Zhu CH, Sheng Y, *et al*. Investigation of mechanical and thermal properties of rare earth pyrochlore oxides by first-principles calculations. *J Am Ceram Soc* 2019, **102**: 2830–2840.
[11] Witte R, Sarkar A, Kruk R, *et al*. High-entropy oxides: An emerging prospect for magnetic rare-earth transition metal perovskites. *Phys Rev Mater* 2019, **3**: 034406.
[12] Rost CM, Sachet E, Borman T, *et al*. Entropy-stabilized oxides. *Nat Commun* 2015, **6**: 8485.
[13] Tsai M-H, Yeh J-W. High-entropy alloys: A critical review. *Mater Res Lett* 2014, **2**: 107–123.
[14] Wei X-F, Liu J-X, Li F, *et al*. High entropy carbide ceramics

from different starting materials. *J Eur Ceram Soc* 2019, **39**: 2989–2994.

[15] Ye BL, Wen TQ, Nguyen MC, *et al*. First-principles study, fabrication and characterization of $(Zr_{0.25}Nb_{0.25}Ti_{0.25}V_{0.25})C$ high-entropy ceramics. *Acta Mater* 2019, **170**: 15–23.

[16] Gild J, Zhang YY, Harrington T, *et al*. High-entropy metal diborides: A new class of high-entropy materials and a new type of ultrahigh temperature ceramics. *Sci Rep* 2016, **6**: 37946.

[17] Qin Y, Liu J-X, Li F, *et al*. A high entropy silicide by reactive spark plasma sintering. *J Adv Ceram* 2019, **8**: 148–152.

[18] Gild J, Braun J, Kaufmann K, *et al.* A high-entropy silicide: $(Mo_{0.2}Nb_{0.2}Ta_{0.2}Ti_{0.2}W_{0.2})Si_2$. *J Materiomics* 2019, https://doi.org/10.1016/j.jmat.2019.03.002.

[19] Gild J, Samiee M, Braun JL, *et al*. High-entropy fluorite oxides. *J Eur Ceram Soc* 2018, **38**: 3578–3584.

[20] Jiang SC, Hu T, Gild J, *et al*. A new class of high-entropy perovskite oxides. *Scripta Mater* 2018, **142**: 116–120.

[21] Dąbrowa J, Stygar M, Mikuła A, *et al*. Synthesis and microstructure of the $(Co,Cr,Fe,Mn,Ni)_3O_4$ high entropy oxide characterized by spinel structure. *Mater Lett* 2018, **216**: 32–36.

[22] Zhang GJ, Zhou L, Li F, *et al.* Synthesis of high entropy ceramic powders for thermal barrier coating. Chinese Patent, Application Number 201910410275.5, May 17 2019.

[23] Subramanian MA, Aravamudan G, Subba Rao GV. Oxide pyrochlores—A review. *Prog Solid State Chem* 1983, **15**: 55–143.

[24] Wang ZJ, Zhou GH, Jiang DY, *et al*. Recent development of $A_2B_2O_7$ system transparent ceramics. *J Adv Ceram* 2018, **7**: 289–306.

[25] Lehmann H, Pitzer D, Pracht G, *et al*. Thermal conductivity and thermal expansion coefficients of the lanthanum rare-earth-element zirconate system. *J Am Ceram Soc* 2003, **86**: 1338–1344.

[26] Murty BS, Yeh JW, Ranganathan S, *et al.* High-entropy alloys: Basic concepts. In: *High-Entropy Alloys*, 2nd edn. Murty BS, Yeh JW, Ranganathan S, *et al.* Eds. Elsevier, 2019: 13–30.

[27] Zhao M, Ren XR, Yang J, *et al*. Low thermal conductivity of rare-earth zirconate-stannate solid solutions $(Yb_2Zr_2O_7)_{1-x}(Ln_2Sn_2O_7)_x$ (Ln = Nd, Sm). *J Am Ceram Soc* 2016, **99**: 293–299.

[28] Cao XQ, Vassen R, Tietz F, *et al*. New double-ceramic-layer thermal barrier coatings based on zirconia–rare earth composite oxides. *J Eur Ceram Soc* 2006, **26**: 247–251.